

## CHARACTERISTICS OF WIND FIELD OVER AN ARTIFICIAL STRAIGHT DUNE AT KASHIMA COAST, JAPAN

Tsukasa Kuribayashi<sup>1</sup>, Keiko Udo<sup>2</sup> and Takanori Uchida<sup>3</sup>

### Abstract

This study conducted Large Eddy Simulation (LES) on wind characteristics around an artificial straight dune which was divided into smaller dunes by aeolian sediment transport during more than ten years at the Kashima Coast. The results show that the time mean wind velocity was found to be large at the top of the dune and small at the lee of the dune when the inflow wind direction was close to vertical to the dune. On the other hand, the mean wind velocity was found to be relatively large at the lee of the dune locally when the inflow wind direction was north and southeast which was close to parallel to the dune. The places where the mean wind velocities were large corresponded to the places where the dune was divided when the inflow wind direction was southeast, but did not correspond when the inflow wind direction was north.

**Key words:** artificial straight dune, LES, coastal dune, characteristics of wind field,

### 1. Introduction

Coastal dunes have a function as an embankment to prevent the intrusion of waves and aeolian sand into the inland as well as having a rich ecosystem. Dune is deformed by drift sand whose external force is wave and by aeolian sand whose external force is wind. There are many studies about aeolian sand on dune (Salmon et al., 1988, Castro et al., 2003, Walker and Nickling, 2003, Baddock et al., 2007, Bechmann and Sørensen, 2010). More studies have been conducted on drift sand compared with aeolian sand in the coastal engineering field because the influence of drift sand on the topography change of dune is larger than aeolian sand in a short term. However, it is indicated by Udo et al. (2003) that the Kashima dune, an artificial straight dune in Ibaraki Prefecture, is eroded from behind and divided into small dunes roughly every 100 m over ten years by the influence of wind. Figure 1(a) shows the aerial photograph of the Kashima dune (provided by Geographical Survey Institute), and Figure 1(b) shows the change of the dune contour from 1984 to 1999 (Udo et al., 2003). It is indicated by Jackson et al. (2011) that wind flow across dunes results in a wide range of turbulent processes at the lee of dune, such as flow separation and reattachment. Long-term deformation of sand dunes impairs their function as an embankment, and the risk of disasters such as tsunami, storm surge and aeolian sand increases. It is necessary to clarify the mechanism of division of dunes and to manage dunes efficiently.

Reynolds Averaged Navier-Stokes (RANS) and LES are often used for numerical calculations of complex topography such as a dune (e.g., Jackson et al., 2011). RANS handles time-averaged fields and does not consider features such as irregular turbulence and vortex structures occurring in complicated topography, whereas LES deals with space-averaged fields and calculates large vortices directly. It was found by Kim and Patel (2000) and Silva Lopes et al. (2007) that the mean wind velocity numerically calculated using LES corresponded better with the measured value in the places where the wind flow decelerates and reverses, than using RANS.

---

<sup>1</sup>International Research Institute of Disaster Science, Tohoku University, 468-1 Aoba, Sendai, Japan.  
tsukasa.kuribayashi.p1@dc.tohoku.ac.jp

<sup>2</sup>International Research Institute of Disaster Science, Tohoku University, 468-1 Aoba, Sendai, Japan.  
udo@irides.tohoku.ac.jp

<sup>3</sup>The Research Institute for Applied Mechanics, Kyushu University, 6-1 Kasuga-koen, Kasuga, Fukuoka, Japan.  
takanori@riam.kyushu-u.ac.jp

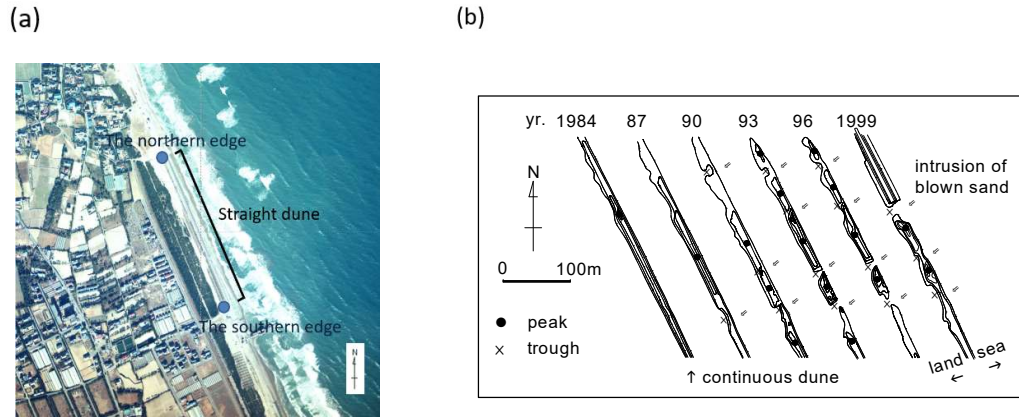


Figure 1. (a) Aerial photographs taken by GSI in 1984 and (b) dune morphology change from 1984 to 1999 (Udo et al., 2003).

The objective of this study is to reproduce wind fields around the straight dune divided into small dunes (Udo et al., 2003), by using LES, aiming to clarify the characteristics of wind field.

## 2. Methods

### 2.1 Wind field analysis model

RIAM-COMPACT® (Uchida, 2014), the numerical fluid analysis software based on LES, was used for the numerical calculations of wind fields. In LES, vortices were divided into two groups, a grid scale group (GS) and a sub grid scale group (SGS) by filtering the turbulent field. GS was calculated directly and SGS influence was modelled. The governing equations, the continuous equation and the Navier-Stokes equation with the filtered flow, were the following equations.

$$\frac{\partial \bar{u}_i}{\partial x_i} = 0 \quad (1)$$

$$\frac{\partial \bar{u}_i}{\partial t} + \bar{u}_j \frac{\partial \bar{u}_i}{\partial x_j} = -\frac{1}{\rho} \frac{\partial \bar{P}}{\partial x_i} + \nu \frac{\partial^2 \bar{u}_i}{\partial x_j \partial x_j} - \frac{\partial \tau_{ij}}{\partial x_j} \quad (2)$$

where  $\bar{u}$  is wind velocity of the filtered flow,  $\rho$  is air density,  $\bar{P}$  is pressure of the filtered flow,  $\nu$  is kinematic viscosity coefficient, and  $\tau_{ij}$  is the deviatoric part of the SGS stress tensor.  $\tau_{ij}$  was modelled with the following standard Smagorinsky model:

$$\tau_{ij} = \frac{1}{3} \overline{u'_k u'_k} \delta_{ij} - 2 \nu_{SGS} \bar{S}_{ij} \quad (3)$$

$$\bar{S}_{ij} = \frac{1}{2} \left( \frac{\partial \bar{u}_i}{\partial x_j} + \frac{\partial \bar{u}_j}{\partial x_i} \right) \quad (4)$$

$$\nu_{SGS} = (C_s f_s D)^2 |\bar{S}| \quad (5)$$

$$|\bar{S}| = (2 \bar{S}_{ij} \bar{S}_{ij})^{1/2} \quad (6)$$

$$\Delta = (h_x h_y h_z)^{1/3} \quad (7)$$

$$f_s = 1 - \exp(-z^+/25) \quad (8)$$

$$z^+ = \frac{zu_*}{\nu} \quad (9)$$

where  $\delta_{ij}$  is Kronecker delta,  $S_{ij}$  is GS component of the strain rate tensor,  $\nu_{SGS}$  is SGS eddy viscosity coefficient,  $f_s$  is characteristic length,  $u_*$  is friction velocity,  $C_s$  is model constant, and  $\Delta$  is mesh size. The characteristic length was used with the decay function method in order to correct the SGS turbulence on the wall.

The convection term of the Navier-Stokes equation was discretized with the third-order accuracy (upwind differencing scheme), and time term, pressure term, and viscosity term were discretized with the second-order accuracy (central differencing scheme).

## 2.2 Calculation condition

The inflow boundary was set to be perpendicular to the inflow wind direction. The inflow wind condition follows the power law of 1/7.

$$V_z = V_R \left( \frac{z}{z_R} \right)^{1/7} \quad (10)$$

where  $V_z$  is the wind velocity at the height  $z$  (m/s),  $V_R$  is the representative wind velocity (m/s), and  $z_R$  is representative length (m). The side boundary surfaces and the upper boundary surface are slip conditions, the outflow boundary surface is a convection type outflow condition, and the ground is a non-slip condition. The dimensionless time increments are  $\Delta t = 1.2 \times 10^{-3}$ , and 50000 steps of numerical calculations are performed. The dimensionless time is  $T^* = 30$  because the simulation handles the latter half of 25000 steps. The dimensionless time  $T^*$  is available by the following equation.

$$T^* = T/(H/U) \quad (11)$$

where  $T$  is the dimensioned time (s),  $H$  is the representative length, and  $U$  is the representative wind velocity. From Equation (11), the time of the numerical calculation is approximately 15 seconds. The representative length is the difference between the maximum elevation and the minimum elevation in the calculation area, and the representative wind velocity is the inflow wind velocity at the height of the maximum elevation.

Typhoon is a tropical cyclone whose maximum wind velocity exceeds 17 m/s. Thus, the representative wind velocity  $u_0$  was set to be 20 m/s.

## 2.3 Target Area

The target area of this study is part of the Kashima dune, which is a straight dune artificially made along the coast from Kashima City to Kamisu City in Ibaraki Prefecture. It was repaired in 2005. The length of the target dune is about 350 m. The coastal forest spreads over the inland side of the dune, and the elevation is higher than at the lee of the dune. In this study, numerical calculations were performed using a digital elevation model of 2 m mesh (Figure 2) measured by the Geographical Survey Institute in 2005. The angle from cross the dune direction is  $\theta$ . The angle of wind vertically traversing the sand dune is  $0^\circ$ .

Distribution of elevation along the top of the dune was extracted from the digital elevation model of 2 m mesh measured by the Geographical Survey Institute in 2005 (Figure 3). The maximum height of the dune top is 9.7 m, the minimum height is 8.7 m, and the standard deviation is 0.16 m. The elevation of top of the dune decreases towards the south slightly with a slope of -0.001.

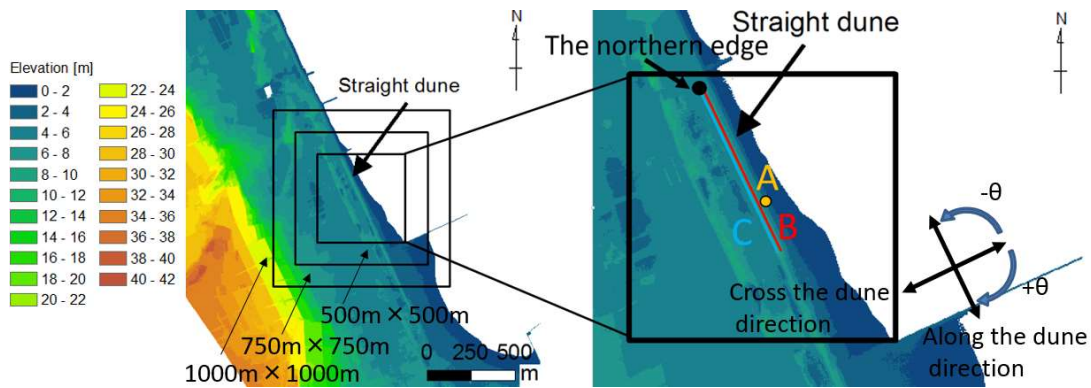


Figure 2. Digital elevation model measured by GSI in 2005.

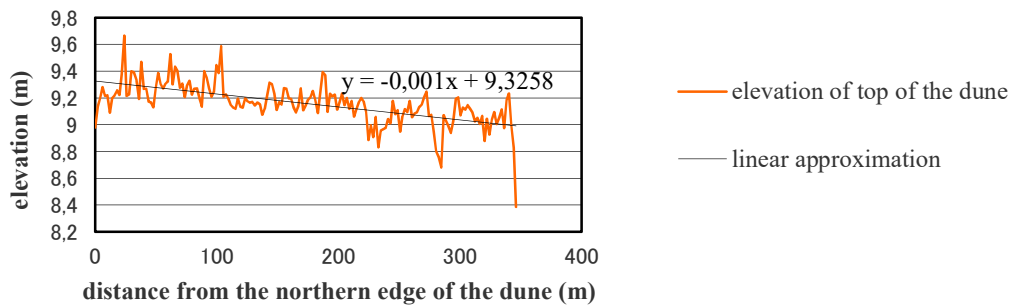


Figure 3. Elevation of the dune

356 points were set at the top and at the lee of the dune (line B and C in Figure 2, respectively) with 1 m intervals and the simulation results for different calculation areas and mesh intervals were compared at the height  $z = 0.17$  so as to decide appropriate conditions. The calculation area and the grid number is 200 m and 50 vertically. The grid number is concentrated near the ground. The mesh interval varies depending on the representative length of the calculation area. For example, the mesh interval is 0.032 to 10 m when the calculation area is 500 m  $\times$  500 m horizontally.

Comparison of calculation areas was performed for three cases: When the area was 500 m  $\times$  500 m, 750 m  $\times$  750 m, and 1000 m  $\times$  1000 m horizontally. The number of grids in the horizontal direction was 500  $\times$  500 at maximum due to the performance of computers. Therefore, the minimum mesh interval of the three cases was 1 m, 1.5 m, and 2 m respectively. Mesh interval of 2 m was used in this comparison.

Comparison of mesh intervals was performed for three cases: When the mesh interval was 1 m, 1.25 m, and 1.67 m. The calculation area of the comparison was 500 m  $\times$  500 m.

Comparison of the calculation area and the mesh interval was performed for two cases: When the inflow wind direction is north-northeast (NNE) and east-southeast (ESE), which are the dominant wind directions of the target area (Figure 4). The changes in the time mean wind velocities of the dimensionless time  $T^* = 30$  at the lee of the dune were compared.

Detailed analysis using appropriate calculation area and mesh interval was performed for seven cases: When the inflow wind was North (N), north-northeast (NNE), northeast (NE), east-northeast (ENE), east (E), east-southeast (ESE), and southeast (SE) considering the dominant wind directions (see Figure 4).

### 3. Results and Discussion

#### 3.1 Determination of calculation area and mesh interval

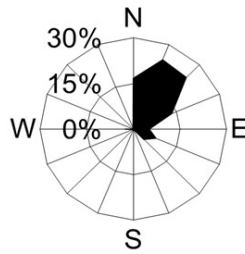


Figure 4. Wind roses during 1985 to 1999 at the Oritsu beach in Ibaraki Prefecture, Japan (Udo et al., 2003).

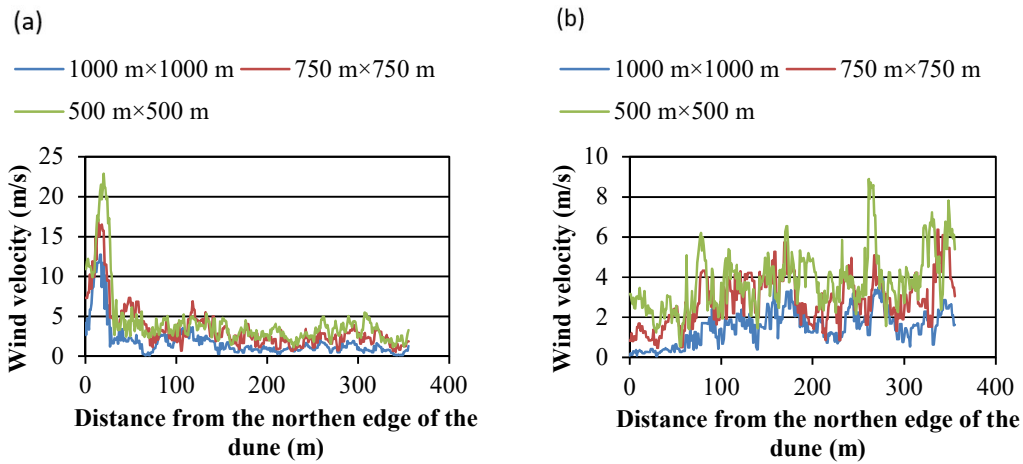


Figure 5. Change in the time mean wind velocity of the dimensionless time  $T^* = 30$  at the lee of the dune in case of three different calculation area when the inflow wind direction is (a) NNE and (b) ESE.

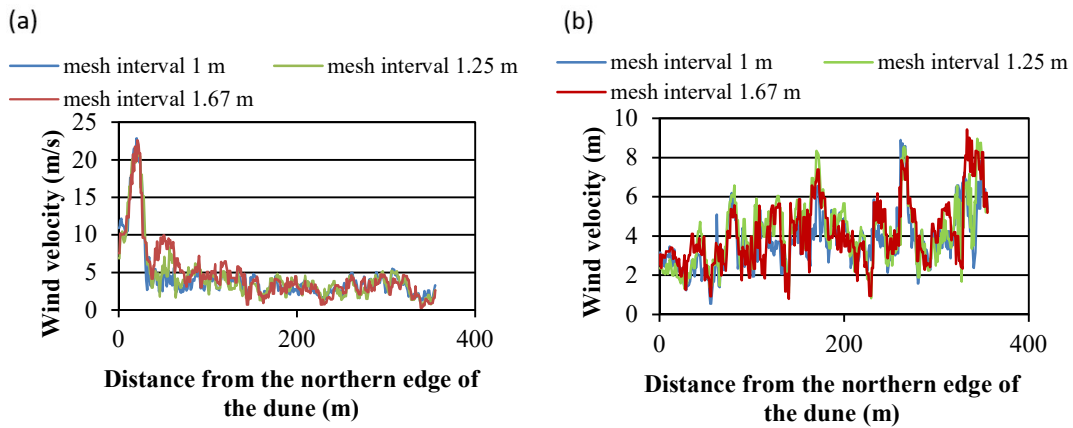


Figure 6. The changes in the time mean wind velocity of the dimensionless time  $T^* = 30$  at the lee of the dune in case of three different mesh intervals when the inflow wind direction was (a) NNE and (b) ESE.

Figure 5 shows the comparison of three different calculation areas. The time mean wind velocity with a small calculation area tended to be large in both cases. However, the trends of the changes were similar.

Figure 6 shows the comparison of three different mesh intervals. The approximate trends were consistent,

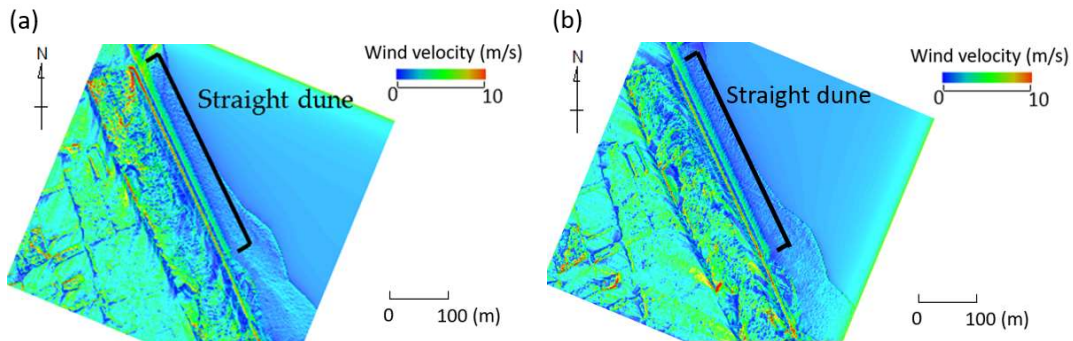


Figure 7. Simulation results of the time mean wind velocity of dimensionless time  $T^* = 30$  when the inflow wind direction is (a) NNE and (b) ESE.

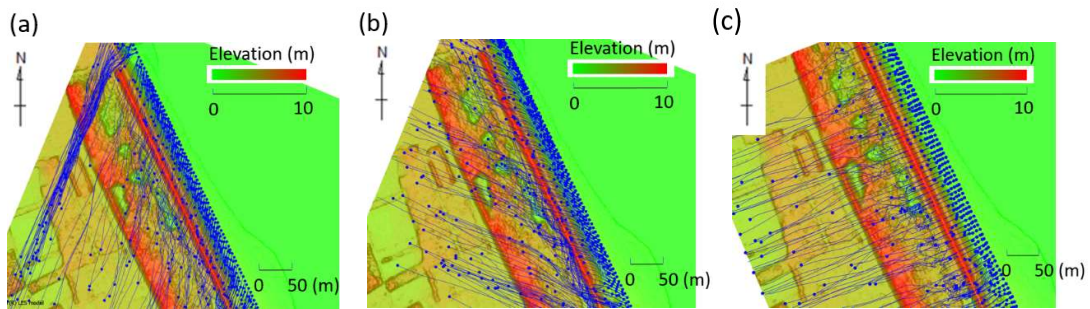


Figure 8. Wind flow when inflow direction is (a) NNE, (b) ESE, and (c) ENE

but there were some different trends locally when comparing the mesh intervals of 1 m and 1.25 m. It was impossible to perform numerical calculations when the grid number was more than  $500 \times 500$  horizontally due to the performance of computer. Therefore, a detailed analysis was performed with the calculation area of  $500 \text{ m} \times 500 \text{ m}$  and the mesh interval of 1 m, the smallest analyzable interval when the calculation area was  $500 \text{ m} \times 500 \text{ m}$ .

### 3.2 Simulation results

Figure 7 shows the simulation results of the time mean wind velocity at a height  $z = 0.07 \text{ m}$  when the inflow wind directions were NNE and ESE. The mean wind velocity increased at the top of the dune and decreased at the lee of the dune when the inflow wind direction was NNE and ESE. The mean wind velocity near northern edge of the dune was larger than other places at the lee of the dune when the inflow wind direction was NNE. On the other hand, that near the southern edge of the dune was larger when the inflow direction was ESE.

Figure 8 shows the wind flow when the inflow wind direction was NNE, ENE and ESE. The wind crossed the dune vertically when the inflow direction was ENE. The wind direction did not change before crossing the dune. The wind flowed south along the lee of the dune when the inflow wind direction was NNE. On the other hand, the wind flowed north along the lee of the dune when the inflow wind direction was ESE. The wind did not flow to a particular direction along the lee of the dune when the inflow wind direction was ENE. It is considered that the wind flowed along the edge of the coastal forest.

### 3.3 Distribution of mean wind velocity and mean wind direction at the top and at the lee of the dune

Figure 9 shows the distribution of the time mean wind velocity and the time mean wind direction at the top and at the lee of the dune in the cases of the seven inflow wind directions.

The mean wind velocity was large at the top of the dune near the northern edge of the dune when the

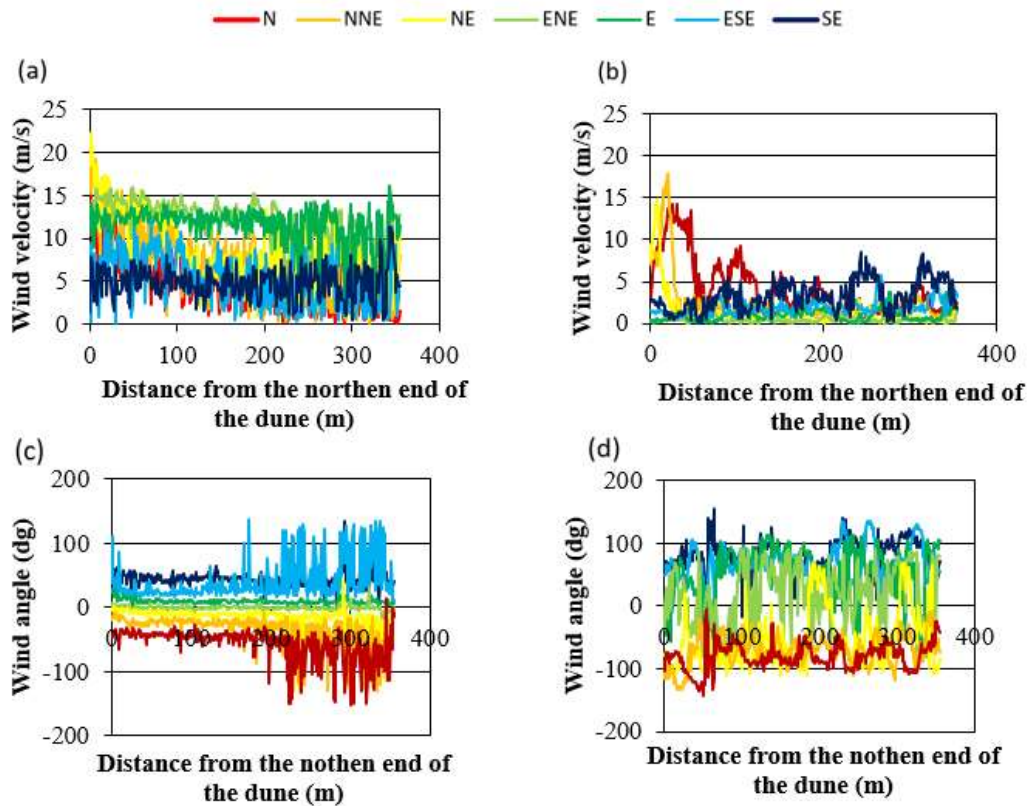


Figure 9. Time mean wind velocity (a) at the top of the dune and (b) at the lee of the dune and the mean wind direction (c) at the top of the dune and (d) at the lee of the dune.

inflow wind direction was N, NNE and NE. On the other hand, the mean wind velocity was large near the southern edge of the dune when the inflow wind direction was E, ESE and SE. The smaller the angle  $\theta$  of the inflow wind direction was, the larger the wind velocity tended to be at the top. The fluctuation of the mean wind velocity became larger in the south part of the dune for all cases.

The fluctuation of mean wind direction at the top of the dune was small in the north part of the dune for all cases, but the fluctuation was large in the south part when the inflow wind direction was other than ENE and E. The wind direction was likely to change due to the influence of the terrain because the mean wind velocity at the top of the dune was relatively small when the inflow wind direction was other than ENE and E.

The smaller the angle  $\theta$  of the inflow wind direction was, the smaller the time mean wind velocity tended to be at the lee of the dune. The wind obliquely crossing the dune has a gentler slope compared with the wind vertically crossing the dune because the distance the wind flows towards the top of the dune is large. The wind is likely to affect the lee of the dune in the case of gentle slope because it does not flow upward but flows near the ground after crossing the dune (Hagino, 2012).

The distribution of the time mean wind velocity at the lee of the dune were different according to the inflow wind direction. The mean wind velocity was large at the lee of the dune near the northern edge of the dune when the inflow wind direction was N, NNE, and NE. The mean wind velocity was large near the southern edge of the dune when the inflow wind direction was E, ESE, and SE. The mean wind velocity was locally very large in the case of N and SE. The wind velocity tended to increase notably nearly every 50 m in the north part of the dune when the inflow wind direction was N, and nearly every 100 m in the whole of the dune when the inflow wind direction was SE.

The tendency of the time mean wind direction at the lee of the dune varied depending on the inflow wind

direction. The smaller the angle  $\theta$  of the inflow wind direction was, the larger the fluctuation of the direction at the lee of the dune was.

### 3.4 Comparison of migration start threshold wind velocity and mean wind velocity

The threshold wind friction velocity is often calculated using the following equation by Bagnold (1941):

$$u_{*t} = A \sqrt{\frac{\rho_s - \rho}{\rho} g d} \quad (11)$$

where  $u_{*t}$  is threshold wind friction velocity,  $\rho_s$  is density of sand ( $2.65 \times 10^3 \text{ kg/m}^3$ ),  $g$  is acceleration of gravity ( $= 9.81 \text{ m/s}^2$ ),  $d$  is particle size of sand, and  $A$  is experiment coefficient ( $= 0.1$ ). The grain size of the sand was set as  $2.0 \times 10^{-4} \text{ m}$  (Udo et al. 2009). Substituting the grain size in the Bagnold's equation gives  $u_{*t} = 0.21 \text{ m/s}$ .

Then, the threshold wind velocity is calculated. This velocity is a wind velocity which generate wind aeolian sand at a certain height. The threshold wind velocity  $u_t$  at a certain height is often calculated using the following equation

$$u_t = \frac{u_{*t}}{\kappa} \ln\left(\frac{z}{z_0}\right) \quad (12)$$

where  $\kappa$  is Karman coefficient ( $= 0.4$ ),  $z$  is calculated height of wind velocity ( $= 0.07 \text{ m}$ ) and  $z_0$  is roughness length ( $= d/30 = 6.7 \times 10^{-6} \text{ m}$ ). Substituting the threshold wind friction velocity in the law gives  $u_t = 4.8 \text{ m/s}$ .

Figure 9(b) shows the comparison of the threshold wind velocity and the time mean wind velocity at the lee of the dune. The wind velocity locally exceeded the threshold wind velocity when the inflow wind direction was N and SE. However, there were few places where the mean wind velocity at the lee of the dune exceeded the threshold wind velocity when the inflow direction is other than N and SE. Therefore, it is considered that N and SE have the great influence on the division of the dune.

### 3.5 Relationship between the mean wind velocity and the mean wind direction at the lee of the dune

Figure 10 shows the relationship between the mean wind velocity and the mean wind direction at the lee of the dune when the inflow wind direction was N and SE, respectively. The mean wind directions were close to parallel to the dune at the lee of the dune where the wind velocities were large., whereas the wind directions were oblique to the dune at the lee of the dune where the wind velocities were small when the inflow wind direction was both N and SE.

### 3.6 Comparison between the places where the wind velocity exceeded the threshold wind velocity and the places where the dune was divided

Figure 11 shows the comparison between the places where the wind velocity exceeded the threshold wind velocity when the inflow wind direction was N and SE respectively and the places where the dune was divided. The places where the dune was divided corresponded to the places where the wind velocity exceeded the threshold wind velocity when the inflow wind direction was SE, whereas did not correspond when the inflow wind direction was N.

## 4. Conclusions

In this study, the wind conditions around the straight coastal dune were reproduced using the numerical fluid analysis software RIAM-COMPACT® based on LES. The obtained results are as follows:

- Time mean wind velocity was large at the top and small at the lee of the dune, and it fluctuated depending

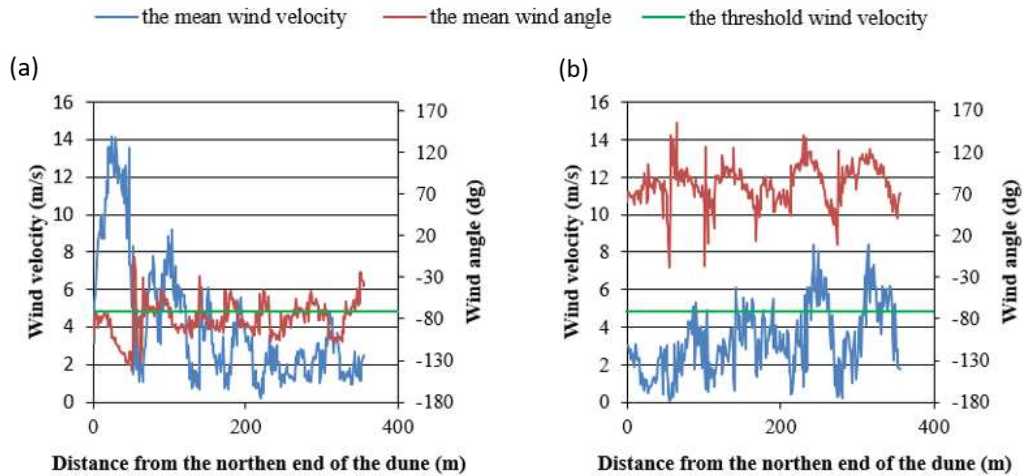


Figure 10. Relationship between the mean wind velocity and the mean wind direction at the lee of the dune when the inflow direction is (a) N and (b) SE.

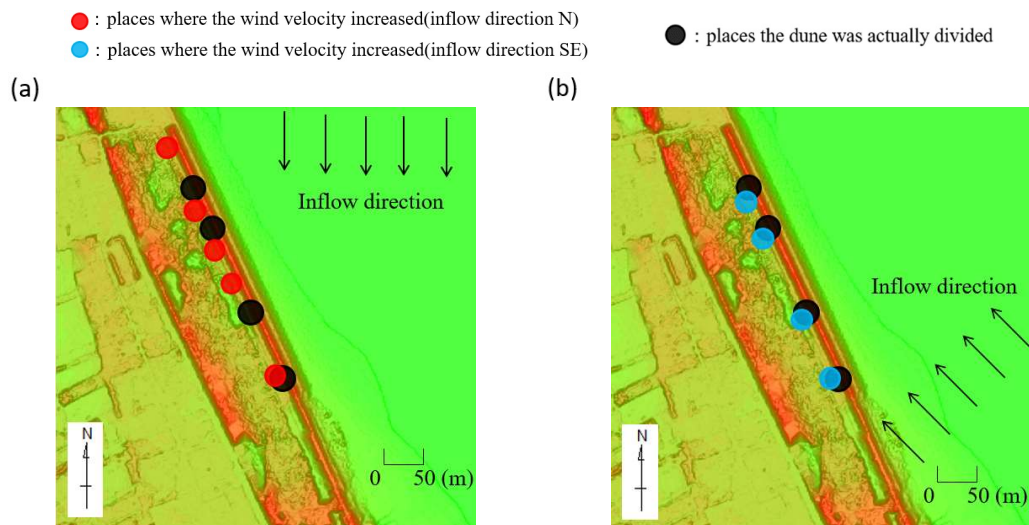


Figure 11. Places where the wind velocity was large when the inflow wind directions are (a) N and (b) SE and the places where the dune is actually divided.

on the inflow wind velocity.

- The time mean wind velocity tended to be large as the angle of the inflow wind direction was close to vertical at the top of the dune. The wind direction relatively fluctuated in the south part of the dune at the top of the dune when the inflow wind direction was N, NNE, NE, ESE, and SE.

- The time mean wind velocity locally tended to be large as the angle of the inflow wind direction was close to parallel to the dune at the lee of the dune. The mean wind direction relatively fluctuated as the inflow wind direction was close to vertical.

- The time mean wind velocities were locally large and exceeded the threshold wind velocity at the lee of the dune when the inflow wind direction was N and SE. The mean wind velocity tended to be large nearly every 50 m in the north part of the dune when the inflow wind direction was N, and it tended to be large nearly every 100 m in the whole of the dune when it was SE. The wind directions at the lee of the dune where the mean wind velocities were large were approximately along the dune direction, whereas the mean wind

directions at the lee of the dune where the wind velocities were small were oblique direction. The places where the velocities exceeded the threshold wind velocity corresponded to the places where the dune was divided when the inflow wind direction was SE, whereas did not correspond when the inflow direction was N.

### Acknowledgements

This work was supported by JSPS KAKENHI Grant Numbers 25420515 and 15KK0223.

### References

- Baddock MC, Livingstone I and Wiggs GFS. 2007. The geomorphological significance of airflow patterns in transverse dune interdunes, *Geomorphology* 87: 322-336
- Bagnold, R.A. 1941. The Physics of Aeolian sand and Desert Dunes, Methuen. London, 265.
- Bechmann A, Sørensen NN. 2010. Hybrid RANS/LES method for wind flow over complex terrain, *Wind Energy*, 13: 36–50.
- Castro, FA., Palma, JMLM., Silva Lopes, A. 2003. Simulations of the Askervein flow, Part 1: Reynolds averaged Navier Stokes equations (k -  $\epsilon$  turbulence model), *Boundary - Layer Meteorology*, 107: 501-530
- Hagino, H. 2012. The Preventive Effect of an Artificial Dune Against Wind and Aeolian sand, *Water science*, 325: 41-49. (in Japanese)
- Jackson, D. W. T., Beyers, J. H. M., Lynch, K., Cooper, J. A. G., Baas, A. C. W. and Delgado-Fernandez, I. 2011. Investigation of three - dimensional wind flow behavior over coastal dune morphology under offshore winds using computational fluid dynamics (CFD) and ultrasonic anemometry, *Earth Surface Processes and Landforms*, 36: 1113-1124.
- Kim H. G. and Patel V. G. 2000. Test of turbulence models for wind flow over terrain with separation and recirculation, *Boundary - Layer Meteorology*, 94: 5–21.
- Nishimura, Y., Minohara, H., and Yanagisawa, A. 2003. Measures to control aeolian sand and changes in sand level in the fore-dune area of the Shonai coastal sand dunes, *Journal of Japanese Society of Coastal Forest*, Vol. 3 (1): 1-5
- Salmon JR, Bowen AJ, Hoff AM, Johnson R, Mickle RE, Taylor PA. 1988. The Askervein hill experiment: mean wind variations at fixed heights above the ground, *Boundary - Layer Meteorology*, 43: 247–271
- Silva Lopes A., Palma J.M.L.M., and Castro F.A. 2007. Simulations of the Askervein flow, Part 2: Large-eddy simulations, *Boundary - Layer Meteorology*, 125: 85-108.
- Uchida, T. 2014. Validation testing of the prediction accuracy of the numerical wind synopsis prediction technique RIAM-COMPACT for the case of the bolund experiment: comparison against a wind-tunnel experiment, *Reports of RIAM, Kyushu University*, 147: 7-14.
- Udo, K., Takewaka, S. and Nishimura, H. 2003. Long-term morphological change of backshore dunes, *Coastal Engineering 2002 (Proc. of 28th Int. Conf. on Coastal Eng.)*: 3786-3798.
- Udo, K., S. Yamawaki, and Y. Ito 2007. Temporal changes of backshore topography and sand grain size under wind and wave actions, *Coastal Engineering 2007 (Proc. of 30th Int. Conf. on Coastal Eng.)*: 2906-2918.
- Udo, K., H. Tanabe, and A. Mano 2009. Short-term sand coarsening process in a backshore between headlands, *Coastal Engineering 2009 (Proc. of 31st Int. Conf. on Coastal Eng.)*: 1901-1913.
- Udo, K., Junaidi, S. Mitsushio, S. Aoki, S. Kato, and A. Mano 2011. Field measurement of Aeolian sand flux using ceramic sand flux sensor UD-101 at a sand dune, *Coastal Engineering 2011 (Proc. of 32nd Int. Conf. on Coastal Eng.)*: 1901-1913.
- Walker IJ, Nickling WG. 2003. Simulation and measurement of surface shear stress over isolated and closely spaced transverse dunes, *Earth Surface Processes and Landforms*, 28 : 1111–1124.